Geophysical Research Letters

RESEARCH LETTER
10.1029/2018GL077325

**Key Points:**
- Ocean dynamics alters the coupled climate response to an abrupt loss of Arctic sea ice loss within 25 years
- Ocean dynamics produces an equatorially symmetric response in the tropics; thermodynamic air-sea coupling causes an antisymmetric response
- Vertical advection tied to warming at depth produces the equatorial Pacific sea surface temperature warming maximum

**Supporting Information:**
- Supporting Information S1

**Correspondence to:**
C. Deser,
cdeser@ucar.edu

**Citation:**
Wang, K., Deser, C., Sun, L., & Tomas, R. A. (2018). Fast response of the tropics to an abrupt loss of Arctic sea ice via ocean dynamics. *Geophysical Research Letters*, *45*, 4264–4272. https://doi.org/10.1029/2018GL077325

Received 30 JAN 2018
Accepted 11 APR 2018
Accepted article online 24 APR 2018
Published online 4 MAY 2018



# Fast Response of the Tropics to an Abrupt Loss of Arctic Sea Ice via Ocean Dynamics

**Kun Wang[1,2,3], Clara Deser[1], Lantao Sun[4], and Robert A. Tomas[1]**

[1]National Center for Atmospheric Research, Boulder, CO, USA, [2]Laboratory for Climate and Ocean-Atmosphere Studies, Department of Atmospheric and Oceanic Sciences, School of Physics, Peking University, Beijing, China, [3]Department of Aviation Meteorology, College of Air Traffic Management, Civil Aviation University of China, Tianjin, China, [4]Cooperative Institute for Research in Environmental Sciences, University of Colorado Boulder and NOAA Earth System Research Laboratory, Boulder, CO, USA

**Abstract** The role of ocean dynamics in the transient adjustment of the coupled climate system to an abrupt loss of Arctic sea ice is investigated using experiments with Community Climate System Model version 4 in two configurations: a thermodynamic slab mixed layer ocean and a full-depth ocean that includes both dynamics and thermodynamics. Ocean dynamics produce a distinct sea surface temperature warming maximum in the eastern equatorial Pacific, accompanied by an equatorward intensification of the Intertropical Convergence Zone and Hadley Circulation. These tropical responses are established within 25 years of ice loss and contrast markedly with the quasi-steady antisymmetric coupled response in the slab-ocean configuration. A heat budget analysis reveals the importance of anomalous vertical advection tied to a monotonic temperature increase below 200 m for the equatorial sea surface temperature warming maximum in the fully coupled model. Ocean dynamics also rapidly modify the midlatitude atmospheric response to sea ice loss.

**Plain Language Summary** The effect of projected Arctic sea ice loss on the global climate system is investigated using a state-of-the-art coupled climate model. This study shows that the tropics respond to the ice loss within two to three decades via dynamical ocean processes and air-sea interaction. This tropical response in turn modifies the atmospheric circulation and precipitation responses over the North Pacific. This fast response indicates that ocean dynamics needs to be represented for an accurate picture of the global impact of Arctic sea ice loss.

## 1. Introduction

A seasonally ice-free Arctic Ocean is expected by midcentury under the "business-as-usual" greenhouse gas emissions scenario (IPCC, 2013), with nearly half of the September ice cover already lost (Perovich et al., 2017). As sea ice disappears, the newly open waters of the Arctic Ocean flux heat and moisture to the overlying atmosphere, warming the lower troposphere and increasing precipitation locally (Deser et al., 2010; Screen & Simmonds, 2010). Remote impacts are also anticipated via changes in the large-scale atmospheric circulation, but this link is more difficult to observe due to confounding influences from internal variability (Barnes & Screen, 2015; Blackport & Kushner, 2016; Sun et al., 2016).

The remote response to ice loss can be isolated in modeling studies provided the ensemble size is large enough to reduce the internal variability. In atmospheric models, this response is largely confined to north of 30°N, while in fully coupled ocean-atmosphere models it spans the full globe (Deser et al., 2015 [D15]). Ocean dynamics play a crucial role in the coupled response, altering the spatial structure and amplitude especially at low latitudes (Tomas et al., 2016 [T16]). An open question is how long it takes for ocean dynamics to modify the coupled response to Arctic sea ice loss, since previous studies focused only on the equilibrium response. (Blackport & Kushner, 2016, compared the high-latitude response at equilibrium with that averaged over the first 50 years but did not investigate the transient evolution in detail.)

The purpose of the present study is to investigate the transient adjustment of the global coupled climate system to a sudden loss of Arctic sea ice loss, with a particular focus on the role of ocean dynamics. To isolate the role of ocean dynamics, we perform two 100-year ensembles of coupled model experiments, each subject to the same Arctic sea ice loss but with different ocean configurations: a thermodynamic slab mixed layer and a full-depth ocean that includes both dynamics and thermodynamics. Here we focus on the evolution of the

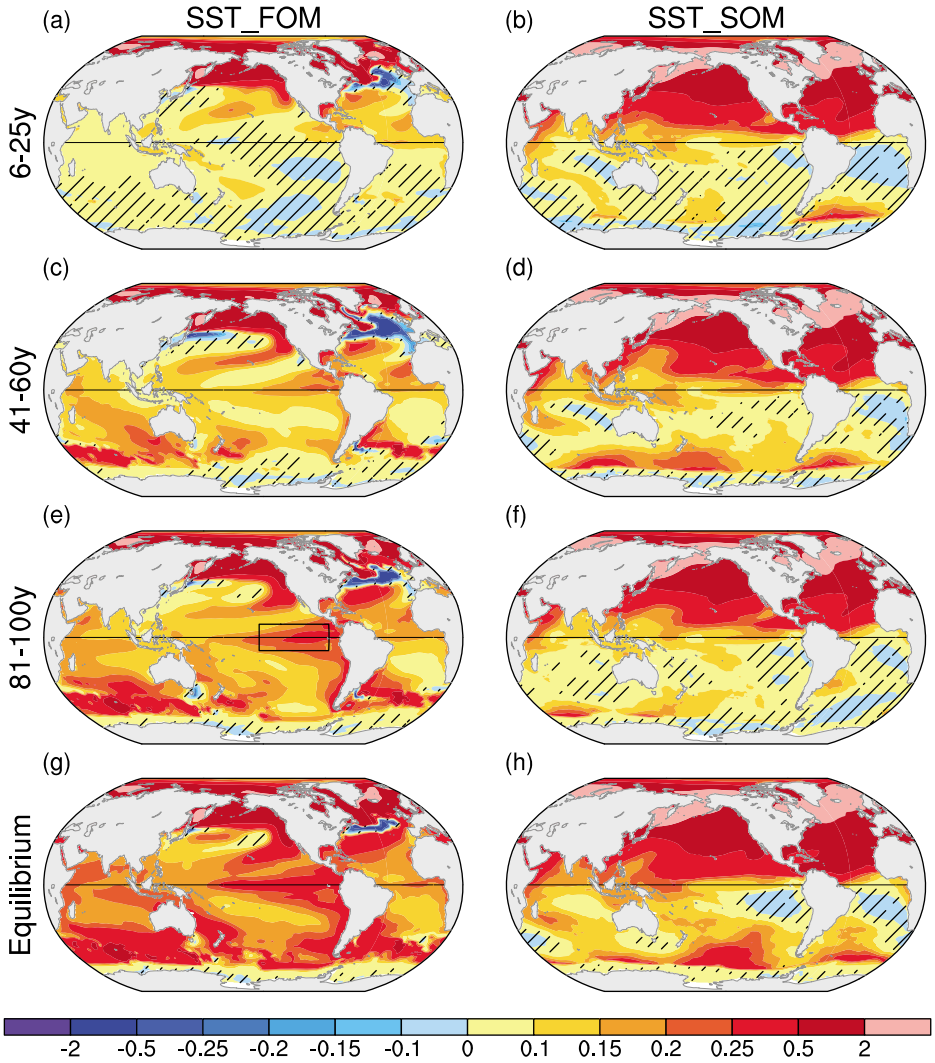


**Figure 1.** Sea surface temperature (SST; °C) responses to an abrupt loss of Arctic sea ice in full ocean model (FOM) and slab-ocean model (SOM) averaged over years (a, b) 6–25, (c, d) 41–60, (e, f) 81–100, and (g, h) 100–360 (equilibrium). Values not significant at the 90% confidence level are hatched.

tropical Pacific coupled response and associated changes over the North Pacific. Our results show that ocean dynamics become important within two decades of a sudden loss of Arctic sea ice, considerably faster than often assumed (Cvijanovic et al., 2017).

## 2. Model and Experiments

The model and experimental design are identical to those in T16 and briefly summarized here. We use the Community Climate System Model version 4 (CCSM4) at 1° horizontal resolution in two ocean configurations: full ocean model (FOM) and slab-ocean model (SOM). SOM has FOM's spatially varying mixed layer depth climatology and a spatially varying "q-flux" so that its sea surface temperature (SST) mean seasonal cycle (1980–1999) matches FOM's. Twenty (10) pairs of 100-year long simulations are conducted with FOM (SOM) under year 2000 radiative forcing; ensemble spread is generated by perturbing the initial atmospheric temperatures by order $10^{-14}$ K. Each pair consists of two different Arctic sea ice states, which approximate those simulated by CCSM4 during 1980–1999 and 2080–2099 under historical and RCP8.5 radiative forcing, respectively. These ice conditions are achieved by adding a seasonally varying longwave radiative flux to the sea ice model at each grid box and time step in the Arctic only; this flux is invisible to the atmosphere and

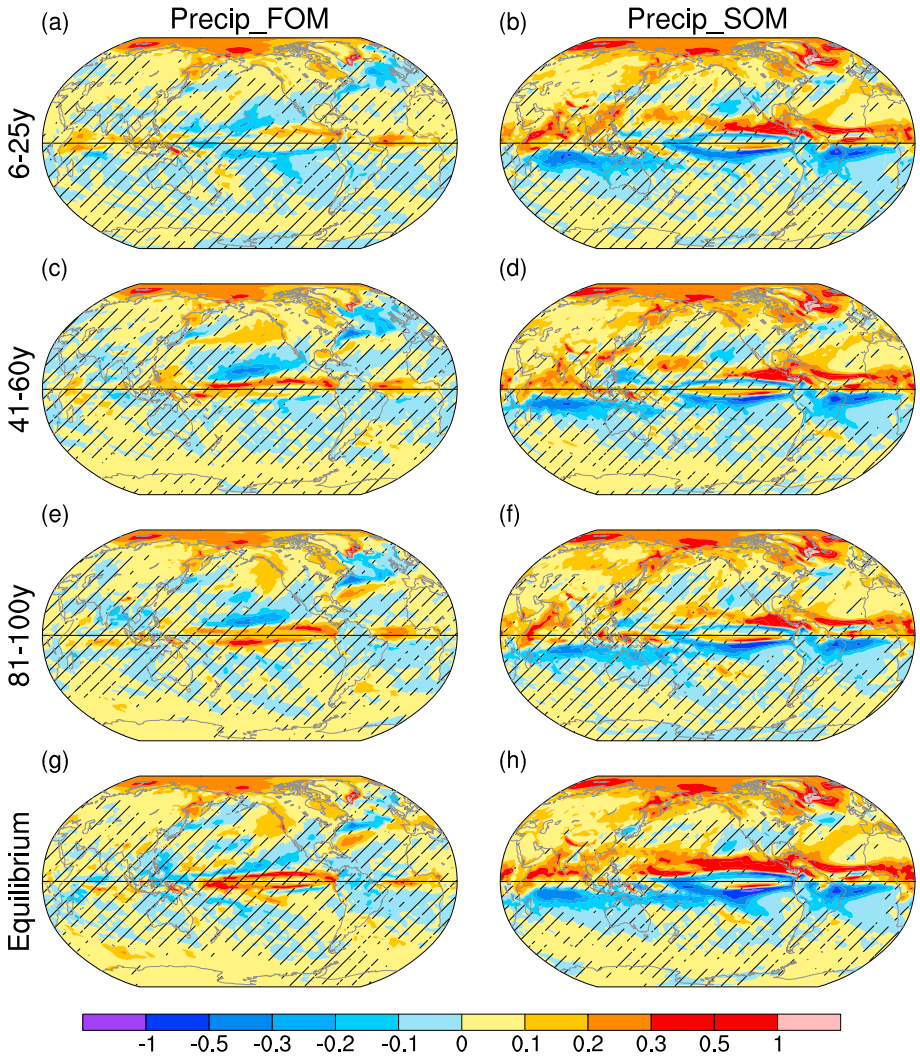


**Figure 2.** As in Figure 1 but for precipitation (mm/day).

ocean. Differencing the paired simulations isolates the coupled response to late 21st-century Arctic sea ice loss relative to present day. Statistical significance is assessed using a two-sided Student's *t* test at the 10% confidence level.

Unlike our ensemble, T16 conducted only a single pair of simulations with FOM and SOM, but theirs were 360 years long, allowing them to analyze the equilibrium portion of the response based on years 100–360. They also demonstrated that the SOM reproduces the FOM's equilibrium response when both the sea ice loss and the heat transport response to that ice loss deduced from the FOM are imposed (the latter by means of a q-flux). Thus, the role of ocean heat transport in the coupled response to sea ice loss may be inferred by comparing the SOM and FOM responses.

## 3. Results

The SST responses in FOM and SOM (Figure 1) show very different evolutions and geographical patterns, depicted by averages over three 20-year periods (years 6–25, 41–60, and 81–100; the first 5 years are omitted while the sea ice is transitioning). The SOM response is dominated by an interhemispheric contrast in all three periods, with significant poleward amplified warming in the Northern Hemisphere (NH) and generally

insignificant changes in the Southern Hemisphere (SH), the high-latitude SH warming in the middle period notwithstanding. The FOM response is more complex, with distinctive patterns that evolve over time. In the North Atlantic, a region of cooling occurs along the path of the Gulf Stream Extension, sandwiched between strong warming in the subpolar gyre and a band of weaker warming in the western subtropical gyre that strengthens over time, as well as a warming center emanating from West Africa. In the North Pacific, large SST increases occur in the subpolar gyre, flanked to the south by a narrow center of cooling along the Kuroshio-Oyashio Extension, as well as a tongue of weaker warming extending from the United States into the western subtropics that strengthens over time. In the tropical Pacific, a well-defined center of warming occurs to the west of Central America in the first time period, but by the middle and later periods, the dominant feature is the eastern equatorial warming maximum that strengthens with time. In the SH, positive SST anomalies develop in the extratropics by the middle period and amplify over time. Further amplification of the SST responses occurs beyond year 100 in both FOM and SOM, as seen by comparing years 81–100 with years 100–360 obtained from the longer (single) pair of simulations conducted by T16, but the patterns remain similar (Figure 1).

Like SST, the precipitation responses in FOM and SOM show very different spatial patterns and temporal evolutions, particularly in the tropics (Figure 2). The tropical rainfall response in SOM is dominated by negative values south of the equator and positive values north of the equator, indicative of a northward displacement of the Intertropical Convergence Zone (ITCZ; Figure 2) and accompanying Hadley Circulation (supporting information Figure S1), with little change in strength over time (although it strengthens beyond 100 years in conjunction with the southward amplification of the SST anomalies to the north of the equator). Embedded within this broad-scale pattern are regional features, including a narrow band of negative values centered a few degrees north of the equator in the Pacific. The pattern of tropical rainfall response in FOM bears little resemblance to that in SOM, especially after year 25. In particular, FOM generally lacks negative precipitation anomalies in the southern tropics, and the near-equatorial Pacific response consists of two narrow bands of positive anomalies centered a few degrees off the equator in the middle and late periods as well as at equilibrium. In addition, negative anomalies are found over the subtropical North Pacific, a feature largely absent in SOM. The amplitude of the tropical precipitation response is generally weaker in FOM than SOM throughout the simulations. Consistent with the rainfall response, FOM shows an equatorward intensification of the Hadley Circulation, especially in the middle and late periods, a pattern that is nearly orthogonal to the northward shift evident in SOM (Figure S1). FOM and SOM also show opposite Walker Circulation responses in the middle and late periods (Figure S2).

The time evolution of zonal mean SST, surface wind, and precipitation responses in FOM and SOM within the tropics is depicted in Figure 3. A 10-year running mean has been applied to reduce the noise from residual interannual El Niño–Southern Oscillation variability. The SST response is shown as the departure from the tropical (30°N to 30°S) mean to highlight the relationship between SST gradients and surface winds. The SOM response shows a simple quasi-stationary pattern of southeasterly wind anomalies south of the equator, southerly anomalies at the equator, and southwesterly anomalies north of the equator, consistent with the pressure-gradient force associated with the anomalous northward SST gradient and the Coriolis force. This leads to anomalous surface wind divergence south of approximately 5°S and convergence to the north (not shown), consistent with reduced precipitation in the latitude band 5°S–30°S and enhanced precipitation in the band 5°S to 30°N. This dipole pattern represents a broad northward shift of the climatological double ITCZ (Figure 3) and Hadley Circulation (Figure S1). The FOM response shows an evolving structure. In the first 20 years, the SST and wind anomalies are not unlike those in SOM, although the northward directed SST gradient and associated surface wind anomalies are weaker (note the different wind vector scales). Around year 20, however, the FOM response departs markedly from the SOM, with the appearance of a narrow band of warming along the equator, which causes northerly wind anomalies to the north (as far as 10°N), resulting in surface wind convergence over the warm equatorial SST maximum and divergence between approximately 10°N–25°N. This pattern persists through the simulation, with a slight broadening of the southern edge of the equatorial SST warming to approximately 10°S after year 75. The FOM precipitation response follows that of the implied surface wind divergence, with increased rainfall in the band 8°S to 8°N and decreased rainfall to the north and south extending to approximately 25°. Thus, the FOM precipitation response differs strikingly from the SOM, even as early as the second decade after an abrupt loss of Arctic sea ice. Analogous results are found for zonal averages restricted to the Pacific sector (Figure S3).

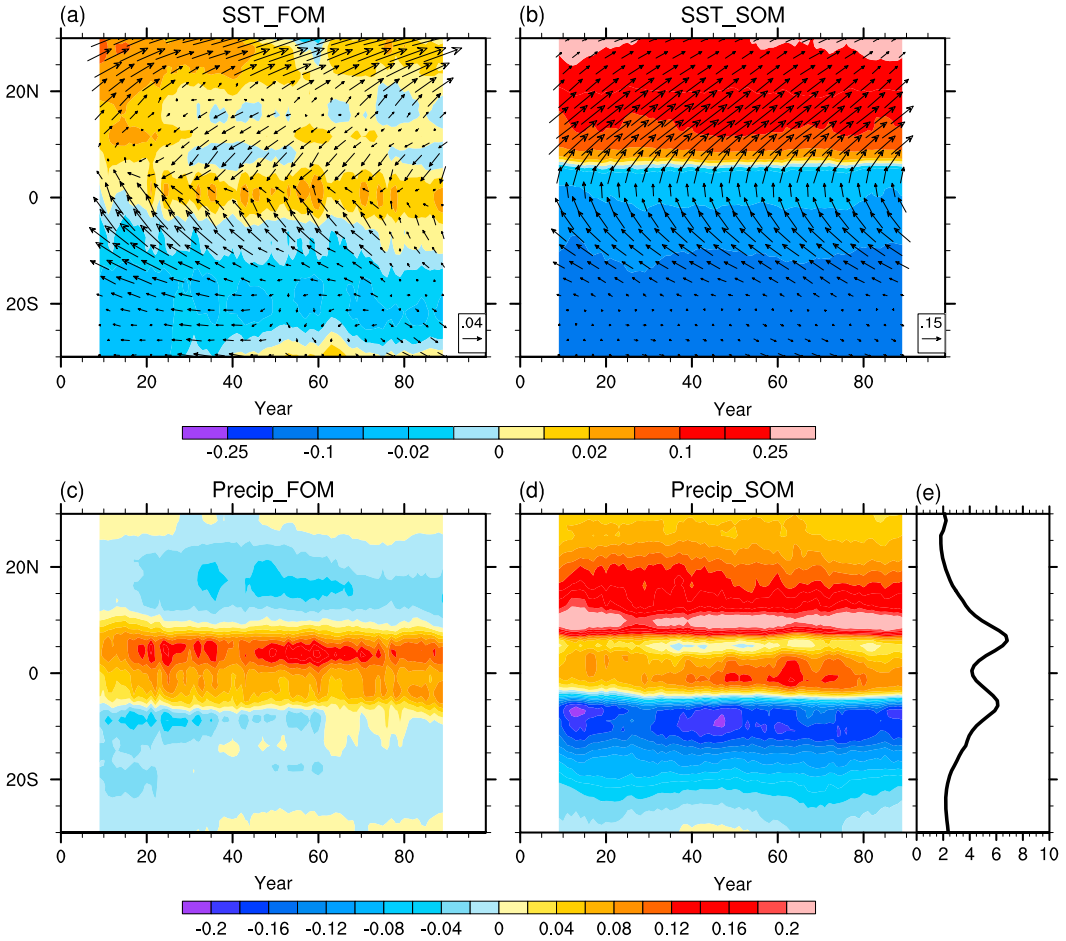


**Figure 3.** Evolution of zonally averaged (a, b) sea surface temperature (SST; °C) and surface wind (m/s) and (c, d) precipitation (mm/day) responses to an abrupt loss of Arctic sea ice in full ocean model (FOM) and slab-ocean model (SOM). (e) Climatological zonal-mean precipitation (mm/day).

A key difference between the two coupled model configurations is the rapid development of a distinct SST warming maximum in the eastern equatorial Pacific approximately two decades after ice loss in FOM, a feature that is absent in SOM. To understand the processes responsible for this equatorial warming maximum, we perform a heat budget analysis following Gaspar et al. (1990) and Redi (1982) for the region 10°S to 10°N, 90°W to 150°W, focusing on the upper 100 m to avoid strong contributions from vertical diffusion and entrainment (Buckley et al., 2014; DiNezio & Deser, 2014). Text S1 provides details of the heat budget calculation. As shown in Figure 4a, the steady increase in temperature averaged over the upper 100 m (T) is due primarily to advection, with a minor contribution from diffusion in the last 20 years, while the net surface heat flux acts as a cooling term. Horizontal advection is the primary warming term in the in the first 25 years (and briefly around year 80), while vertical advection dominates during the remainder of the simulation (Figure 4b).

The vertical advection term can be subdivided into a term related to the anomalous vertical velocity acting on the mean stratification and a term related to the mean vertical velocity acting on the anomalous vertical temperature gradient (the term related to the anomalous vertical velocity acting on the anomalous vertical temperature gradient is negligible; Figure 4c). The first term contributes to warming during years 25–70 and cooling thereafter (Figure 4c), the latter likely a result of anomalous wind convergence and downwelling (Figure S4c). The warming effect of the second term steadily increases in importance after year 25 in association with the pronounced warming at depth, with maximum values between 200 and 400 m (Figure 4c); this subsurface warming is more than twice as large as that in the upper 100 m by

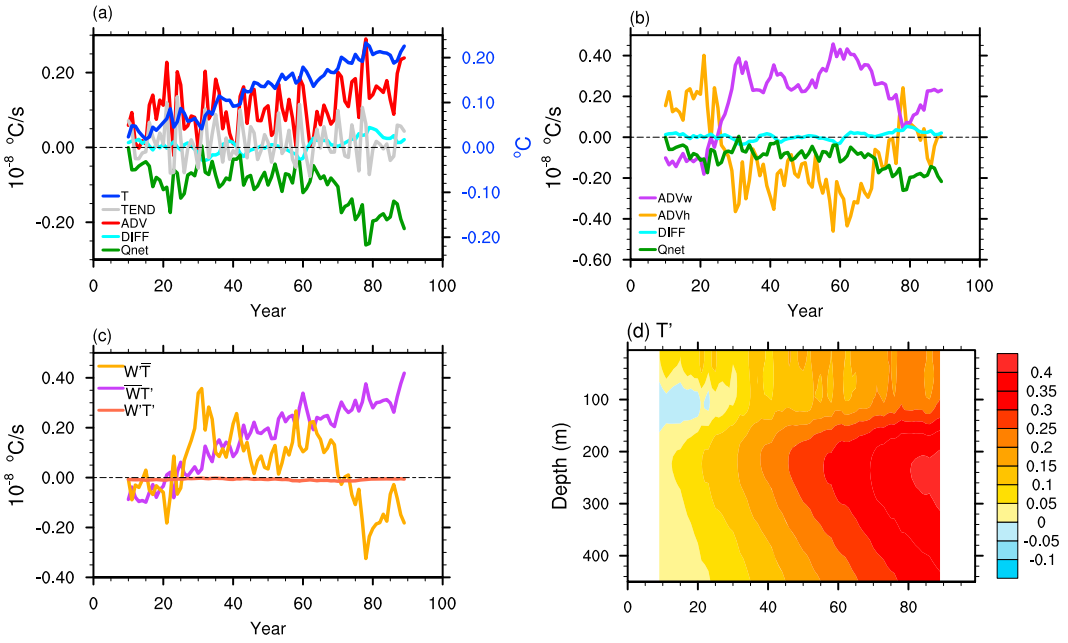


**Figure 4.** Evolution of the eastern equatorial Pacific response to an abrupt loss of Arctic sea ice in full ocean model (FOM). (a–c) Upper 100 m *T* (°C) and heat budget terms (°C/s; defined in Text S1); (d) *T*(*z*). Region outlined in Figure 1e.

year 100 (Figure 4d). Mean upwelling brings this subsurface thermal anomaly into the mixed layer starting around year 30, as evidenced by the vertical connection of the anomalies. Before this time, the warming in the upper 50–70 m is largely disconnected from the subsurface, consistent with the dominance of horizontal advection in the heat budget (Figure 4b).

A heat budget analysis for the 200- to 400-m layer reveals that the subsurface warming is mainly caused by anomalous downwelling and northward flow (Figure S5). The equatorial subsurface warming is part of a larger-scale warming that maximizes between 30°S and 10°S (Figure S6) and which results from anomalous downwelling linked to anomalous Ekman pumping (Figure S7). We note that the associated depression of the 26.5-kg/m$^3$ isopycnal surface (Figure S6) is consistent with the response to a weakened Atlantic Meridional Overturning Circulation (AMOC; Timmermann et al., 2005). In our experiments, AMOC decreases by 6 Sv within the first 20 years of ice loss, followed by a partial recovery to −4.5 Sv by year 100 (Figure S8), representing approximately one-third of the total AMOC decline under RCP8.5 in CCSM4.

During the first 30 years, the increase in the regional temperature index reflects warming to north of the equator rather than along the equator per se (recall Figure 1). This initial warming west of Central America is likely the result of a weakening of the local trade winds (i.e., southwesterly wind anomalies) in response to amplified SST warming in the Caribbean and Gulf of Mexico (Figure S4a). A similar mechanism has been invoked to explain observed tropical SST changes over the past three decades (Li et al., 2016). However, in the case of observations, tropical Atlantic warming also induces easterly wind anomalies over the Indian Ocean and western Pacific, which in turn cause SSTs in the eastern tropical Pacific to cool as a result of the Bjerknes ocean dynamic feedback mechanism. Thus, the warming at 200- to 400-m depth in response to Arctic sea ice loss plays a crucial role in determining the sign of the SST response in the eastern tropical Pacific. In this regard, our results are more in line with those of Zhang and Delworth (2005) who showed that a weakening of AMOC induced by an imposed freshwater forcing causes a warming of the eastern tropical Pacific through air-sea interactions. However, in the case of a weakened AMOC, both the North Atlantic and North Pacific cool, opposite to the warming seen in our sea ice loss experiments which contain both the influence of a reduced AMOC and the larger influence of heat released to the atmosphere from the newly open waters of the Arctic Ocean that is transported southward to warm the oceans (see D15 and T16 for further discussion). Thus, neither recent observed tropical trends nor AMOC changes in isolation provide a good analog for the coupled response to Arctic sea ice loss.

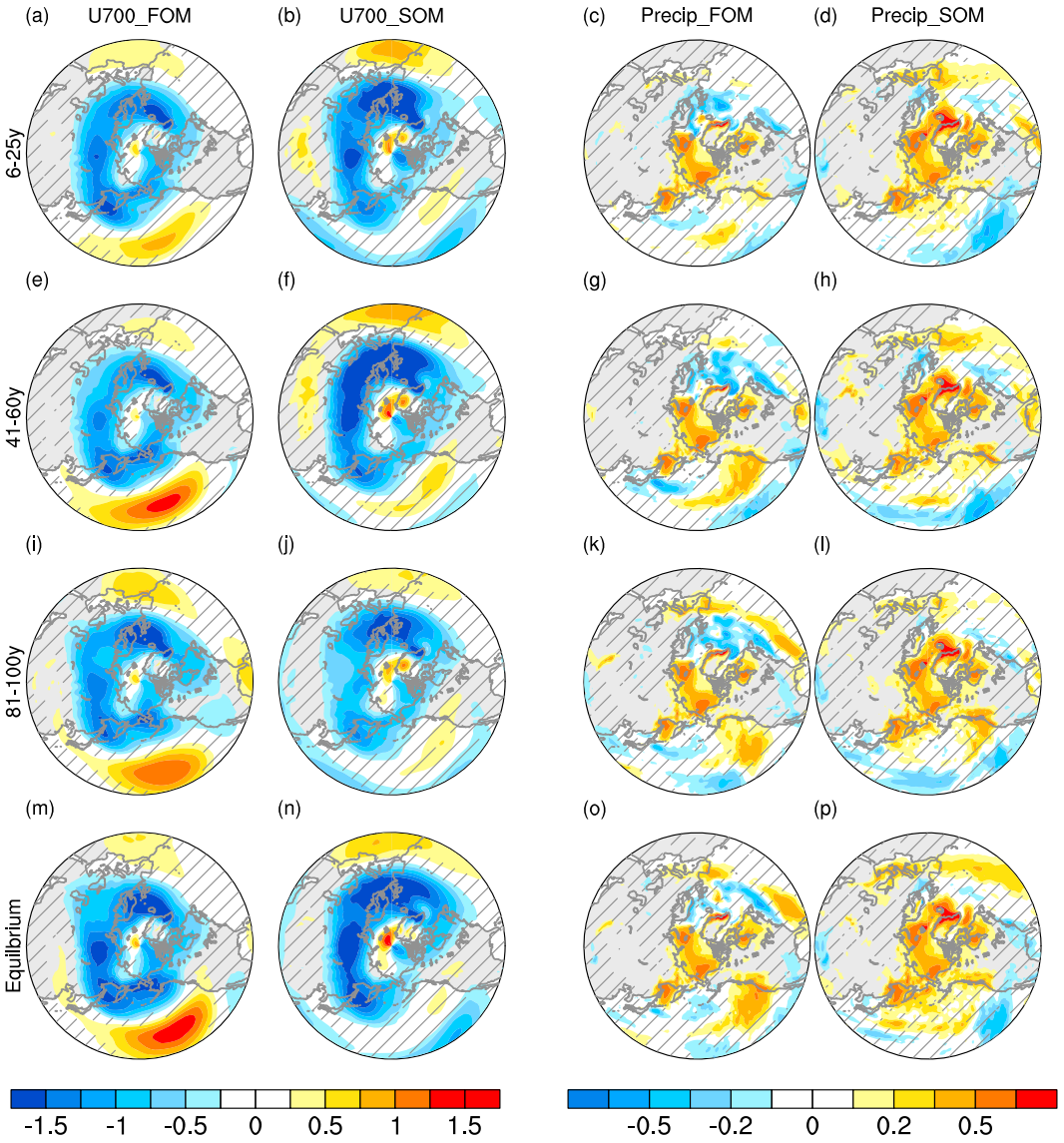


**Figure 5.** As in Figure 1 but for December–February (a, b) U700 (m/s) and (c, d) precipitation (mm/day).

We conclude our analysis of the transient response of the coupled climate system to an abrupt loss of Arctic sea ice by showing the evolution of 700-hPa zonal winds (U700) and precipitation over the extra-tropical NH in December–February (Figure 5; annual means are similar but with reduced amplitude). Both FOM and SOM show a quasi-steady ring of negative U700 at high latitudes (50°N–70°N) on the poleward flank of the eddy-driven jet, which is directly associated with the reduced meridional temperature gradient resulting from warming of the Arctic lower troposphere. However, the midlatitude U700 responses differ, especially in the Pacific where FOM shows large positive values on the equatorward side of the jet (25°N–45°N) that develop in concert with the tropical Pacific SST/rainfall anomalies (recall Figures 1 and 2). In SOM, this feature is considerably weaker, generally insignificant and shifted northward (indeed, SOM shows negative U700 in the latitude band 20°N–35°N). These differences between FOM and SOM appear within the first 25 years and can be traced to their distinctive tropical SST/rainfall responses via Rossby wave dynamics (see T16 for experimental evidence) and to their opposing subtropical meridional SST anomaly gradients via thermal wind balance (Deser et al., 2016).

The extratropical precipitation responses evolve in concert with the U700 responses (Figure 5). In particular, the stronger and southward extended band of westerly wind anomalies over the Pacific in FOM compared to

SOM is generally associated with a larger and broader swath of increased precipitation that reaches into the west coast of North America, with weaker precipitation deficits farther south. Like U700, these differences between FOM and SOM are already evident in the first 25 years, although there is more noise in the evolution of the precipitation response than in the U700 response. The contrasting amplitudes and latitudinal structures of the FOM and SOM precipitation responses are especially clear at equilibrium, not only in the Pacific sector but also over the Atlantic where a local signature of the different SST responses in the vicinity of the Gulf Stream is evident.

## 4. Summary and Discussion

Whereas previous modeling studies have examined the equilibrium coupled climate response to projected Arctic sea ice loss, we have investigated aspects of the transient adjustment to an abrupt loss of Arctic sea ice, with a particular focus on the tropics and the role of ocean dynamics. To study the relative roles of dynamical versus thermodynamic air-sea interaction, we conducted identical sets of experiments with CCSM4 in the full-depth ocean model (FOM) and slab ocean model (SOM) configurations. The SOM response is dominated by a quasi-steady interhemispheric SST contrast (warming in the NH and little change in the SH), accompanied by a northward shift of the ITCZ and Hadley Circulation. The FOM response is more complex, with distinctive patterns that evolve over time. The tropical SST response is characterized by a distinct equatorial Pacific maximum, which develops within approximately 20 years, accompanied by an equatorward intensification of the ITCZ and Hadley Circulation. These structures amplify with time and are in marked contrast to the SOM response. A heat budget analysis for the upper 100 m of the eastern equatorial Pacific indicates the importance of anomalous vertical advection, which is tied to a monotonic warming at depth (below 200 m). Although further diagnostics and experiments are needed to understand the origins of this subsurface warming, it appears to be qualitatively consistent with the adjustment of the global thermohaline circulation to a density perturbation in the North Atlantic, in this case induced by a freshening and warming of the subpolar gyre due to sea ice melt.

In addition to distinctive tropical responses, FOM and SOM also exhibit some differences in their NH midlatitude atmospheric circulation responses. In particular, FOM shows an increase in lower tropospheric westerlies over the North Pacific, a response that strengthens over time. This aspect is very weak and shifted poleward in SOM compared to FOM. In addition, SOM shows reduced westerlies farther south, a feature that is lacking in FOM. These distinctions in the midlatitude circulation responses between FOM and SOM, apparent even within the first 25 years, can be traced to differences in their tropical Pacific SST responses and affect the precipitation response along the west coast of North America among other regions.

In summary, the coupled ocean-atmosphere response to an abrupt loss of Arctic sea ice is rapidly (within 20–30 years) and markedly modified by dynamical ocean processes. To what extent our results depend on the particular model used and the experimental design remains to be ascertained.

**Acknowledgments**
The first author was supported by the Chinese National Science Foundation (NSF) (grants 41376007 and 91337106). NCAR is sponsored by the U.S. NSF. Model data are available on the Earth System Grid (www.earthsystemgrid.org). We thank the two anonymous reviewers for constructive comments.

## References

Barnes, E. A., & Screen, J. A. (2015). The impact of Arctic warming on the midlatitude jet-stream: Can it? Has it? Will it? *WIREs Climate Change*, *6*(3), 277–286. https://doi.org/10.1002/wcc.337

Blackport, R., & Kushner, P. J. (2016). The transient and equilibrium climate response to rapid summertime sea ice loss in CCSM4. *Journal of Climate*, *29*(2), 401–417. https://doi.org/10.1175/jcli-d-15-0284.1

Buckley, M. W., Ponte, R. M., Forget, G., & Heimbach, P. (2014). Low-frequency SST and upper-ocean heat content variability in the North Atlantic. *Journal of Climate*, *27*(13), 4996–5018. https://doi.org/10.1175/jcli-d-13-00316.1

Cvijanovic, I., Santer, B. D., Bonfils, C., Lucas, D. D., Chiang, J. C., & Zimmerman, S. (2017). Future loss of Arctic sea-ice cover could drive a substantial decrease in California's rainfall. *Nature Communications*, *8*(1), 1947. https://doi.org/10.1038/s41467-017-01907-4

Deser, C., Sun, L., Tomas, R. A., & Screen, J. (2016). Does ocean coupling matter for the northern extratropical response to projected Arctic sea ice loss? *Geophysical Research Letters*, *43*, 2149–2157. https://doi.org/10.1002/2016GL067792

Deser, C., Tomas, R., Alexander, M., & Lawrence, D. (2010). The seasonal atmospheric response to projected Arctic sea ice loss in the late twenty-first century. *Journal of Climate*, *23*, 333–351. https://doi.org/10.1175/2009JCLI3053.1

Deser, C., Tomas, R. A., & Sun, L. (2015). The role of ocean–atmosphere coupling in the zonal-mean atmospheric response to Arctic sea ice loss. *Journal of Climate*, *28*(6), 2168–2186. https://doi.org/10.1175/jcli-d-14-00325.1

DiNezio, P. N., & Deser, C. (2014). Nonlinear controls on the persistence of La Niña. *Journal of Climate*, *27*(19), 7335–7355. https://doi.org/10.1175/jcli-d-14-00033.1

Gaspar, P., Grégoris, Y., & Lefevre, J. M. (1990). A simple eddy kinetic energy model for simulations of the oceanic vertical mixing: Tests at station Papa and long-term upper ocean study site. *Journal of Geophysical Research*, *95*(C9), 16,179–16,193. https://doi.org/10.1029/JC095iC09p16179

IPCC (2013). *Climate Change 2013: The Physical Science Basis. Contribution of Working Group I to the Fifth Assessment Report of the Intergovernmental Panel on Climate Change*. In T. F. Stocker, et al. (Eds.) (1535 pp.). Cambridge, UK and New York, NY: Cambridge University Press. https://doi.org/10.1017/CBO9781107415324

Li, X., Xie, S.-P., Gille, S. T., & Yoo, C. (2016). Atlantic-induced pan-tropical climate change over the past three decades. *Nature Climate Change*, *6*, 275–279. https://doi.org/10.1038/nclimate2840

Perovich, D., Meier, W., Tschudi, M., Farrell, S., Gerland, S., Hendricks, S., et al. (2017). Sea ice cover [in state of the climate in 2016]. *Bulletin of the American Meteorological Society*, *98*, S131–S133.

Redi, M. H. (1982). Oceanic isopycnal mixing by coordinate rotation. *Journal of Physical Oceanography*, *12*(10), 1154–1158. https://doi.org/10.1175/1520-0485(1982)012%3C1154:OIMBCR%3E2.0.CO;2

Screen, J. A., & Simmonds, I. (2010). The central role of diminishing sea ice in recent Arctic temperature amplification. *Nature*, *464*(7293), 1334–1337. https://doi.org/10.1038/nature09051

Sun, L., Perlwitz, J., & Hoerling, M. (2016). What caused the recent "warm Arctic, cold continents" trend pattern in winter temperatures? *Geophysical Research Letters*, *43*, 5345–5352. https://doi.org/10.1002/2016GL069024

Timmermann, A., An, S.-I., Krebs, U., & Goosse, H. (2005). ENSO suppression due to weakening of the North Atlantic thermohaline circulation. *Journal of Climate*, *18*(16), 3122–3139. https://doi.org/10.1175/jcli3495.1

Tomas, R. A., Deser, C., & Sun, L. (2016). The role of ocean heat transport in the global climate response to projected Arctic sea ice loss. *Journal of Climate*, *29*(19), 6841–6859. https://doi.org/10.1175/jcli-d-15-0651.1

Zhang, R., & Delworth, T. L. (2005). Simulated tropical response to a substantial weakening of the Atlantic thermohaline circulation. *Journal of Climate*, *18*(12), 1853–1860. https://doi.org/10.1175/jcli3460.1